Carrier Concentration Dependence of Superconducting Gap of $Bi_2(Sr,La)_2CuO_{6+\delta}$

Hideki Sakamoto[1], Koto Ogawa[1], Takeshi Kondo[2], Shik Shin[2], Masaharu Matsunami[3], Hiroshi Ikuta[1], Tsunehiro Takeuchi[3,4]

1. Department of Crystalline Materials Science, Nagoya University, Nagoya 464-8603, Japan.

2. Institute for Solid State Physics, the University of Tokyo, Kashiwa, Chiba 277-8581, Japan.

3.Energy Materials Laboratory, Toyota Technological Institute, Nagoya 468-8511, Japan.

4. Precursory Research for Embryonic Science and Technology Japanese Science and Technology Agency, Tokyo 102-0076, Japan.

Abstract

Carrier concentration dependence of the superconducting gap observable around the nodal region was investigated in detail for a series of high-T_c cuprate superconductors, $Bi_2(Sr,La)_2CuO_{6+\delta}$, by means of ultra-high-resolution laser-induced angle resolved photoemission spectroscopy. We found that the gap can be expressed by the simple *d*-wave gap form, $\Delta = \Delta_0\cos(2\theta)$, at least around the node even in the heavily underdoped samples. The gap size Δ_0 increases with decreasing hole concentration in the overdoped region, and starts to decrease after taking a plateau that extends over a relatively wide hole concentration, p, ranging $0.16 \leq p \leq 0.26$. The critical temperature of superconductivity, T_c, decreases more drastically than Δ_0 with decreasing hole

concentration. This fact indicates that T_c is not simply determined by Δ_0, and we argue that the reduction of T_c with decreasing hole concentration in the underdoped regions is caused by a synergy effect of the decreasing Δ_0 and the development of pseudogap.

1. Introduction

The relation between the pseudogap that develops around the anti-nodal region of the Fermi surface and the stability of superconducting state had been intensively discussed.[1-6] Some experimental results supported the scenario of the pseudogap being a pre-formed superconducting gap,[7-12] which is called as the "one-gap scenario". However, many other experiments suggested that the pseudogap is caused by an unidentified mechanism that is different from the Cooper-pair formation one and prevents the electrons near the anti-nodal region from forming the Cooper pairs.[13-22] The electrons near the node, on the other hand, are not affected by the pseudogap, and the Bose condensation of the Cooper pairs still takes places to stabilize the superconducting state. This idea is called as "two-gap scenario".

Despite a huge number of investigations being performed, the collective excitation leading to the formation of Cooper-pairs has not been fully identified yet. In order to gain deeper insight into the collective excitation, it is of great importance to know the temperature, momentum, and carrier concentration dependences of the superconducting gap because it is directly related with the superfluid density that is known as the order-parameter of superconducting phase. Unfortunately, however, the pseudogap that develops at the underdoped side of the phase diagram has made a detailed study of the superconducting gap for wide range of concentration difficult.

Once the two-gap scenario mentioned above is accepted, one may naturally realized that the superfluid density would not be simply determined by the superconducting gap but also by how wide the momentum range of Fermi surface is. In other words, the

number of Cooper pairs is drastically reduced under the influence of pseudogap, and hence the superconducting critical temperature is also significantly reduced in the underdoped region.

Despite the importance of the relation between the superconducting gap and the pseudogap, the relation between the carrier concentration dependence of superconducting gap and T_c at the underdoped region has not been fully investigated yet because the pseudogap covers a very wide momentum range of Fermi surface. The superconducting gap persists only in a limited range in the vicinity of the node where the superconducting gap has a very small value. Notably, the size of the superconducting gap near the node is generally smaller than the energy resolution of angle resolved photoemission spectroscopy measurements (ARPES) equipped with Vacuum Ultra Violet (VUV) source.

In this study, therefore, we carefully investigated the very small superconducting-gap persisting near the nodal region for a series of $Bi_2(Sr,La)_2CuO_{6+\delta}$ superconductors of various hole concentrations by employing ultra-high-energy-resolution laser induced ARPES measurements (Laser-ARPES),[23]. The shape of the Fermi surface and the size of the pseudogap were also investigated and carefully analyzed by additionally employing the synchrotron radiation ARPES measurements. The hole concentrations for some of the samples were directly estimated from the area enclosed by the Fermi surfaces, using the Luttinger Sum rule. The relations between the pseudogap $\Delta_{PG}(p)$, the superconducting gap $\Delta_0(p)$ and $T_c(p)$ are discussed in terms of carrier concentration.

2. Experiments

$Bi_2(Sr_{1-x}La_x)_2CuO_{6+\delta}$ (La-Bi2201) single crystals were grown by floating-zone (FZ) technique. The detailed information about the sample preparation was reported elsewhere.[24] The single crystals were cut into pieces typically ~1 × 1 × 0.05 mm^3 in dimension. Hole concentration, p, was controlled by both the partial substitution of La for Sr and the subsequent heat treatment (i.e., oxygen content).

Seebeck coefficient $S(T)$ of the samples were measured from 10 to 300 K using a home-made probe that was put in a Physical Properties Measurement System (PPMS) manufactured by Quantum Design Inc.[25] The magnetic susceptibility $\chi(T)$ was also measured over the temperature range from 5 to 35 K using the SQUID magnetometer assembled in the Magnetic Properties Measurement System of Quantum Design Inc. The critical temperature T_c of the superconducting state was determined from the temperature where the susceptibility χ extrapolated from lower temperatures intersected the $\chi = 0$ axis (see Fig. 1b).The samples are labeled according to the doping state and T_c in this paper. For instance, UD11, OP32 and OD23 represent an underdoped sample with T_c = 11 K, the optimally doped one with T_c = 32 K, and the overdoped one with T_c = 23 K, respectively.

The ultra-high-energy-resolution ARPES spectra of the samples were accumulated using the Scienta R4000 hemispherical analyzer coupled with a low energy laser ($h\nu$ = 6.994 eV) at Institute of Solid State Physics (ISSP), the University of Tokyo.[23] The measurements were performed at low temperatures below 6 K that is well lower than T_c of all samples. Although the momentum area measurable in the laser-ARPES is smaller

than the first Brillouin zone, the Fermi momenta around the nodal region, where the superconducting gap opens below T_c, were sufficiently covered by it. The highest energy resolution of the employed ARPES system is ~ 360 μeV, but we used slightly lower energy resolution of 700 μeV for ARPES measurement to obtain larger photoemission signal.

We also carried out synchrotron radiation ARPES measurements at BL-7U UVSOR-II, Okazaki for evaluating the area surrounded by the Fermi surface and the energy-width of pseudogap that opens in the vicinity of $\boldsymbol{k}$ = (π, 0). The measurements were performed with incident photon of 20 eV at 15 K. The total energy resolution of synchrotron-radiation-ARPES was ~10 meV.

3. Results

Figures 1a,b show the Seebeck coefficient and magnetic susceptibility of the samples used in the present work. The observed data are in good consistency with the previously reported results,[24,26] assuring that the quality of the samples was good enough to investigate the carrier concentration dependence of superconducting gap. The magnitude of Seebeck coefficient is known to have a close relation to the hole concentration,[27] and gradually increases with decreasing hole concentration at any given temperature.

Figures 2a–c show the mapping image of ARPES intensity for OD23, UD31 and UD25 at 15 K obtained by the integration of synchrotron-ARPES intensity over the narrow energy range of 10 meV centered at the chemical potential, μ. The large hole-like Fermi surface centered at (π, π) was clearly observed together with that of

umklapp bands[28] caused by the structure modulation at the Bi-O layer. We plotted the hole concentration p, which was estimated from the area surrounded by Fermi surface as a function of Seebeck coefficient observed at 290 K, $S(290)$, in Fig. 2d. An almost linear relation was observable between p and $S(290)$. The hole concentrations of the remaining samples which were not measured by synchrotron ARPES were estimated from $S(290)$ using the obtained relation between p and $S(290)$. Note here that the Luttinger sum rule was reported to be valid in the cuprate superconductors.[29]

We also investigated the magnitude of pseudogap from synchrotron ARPES measurement. The energy distribution curves (EDCs) at the Fermi momentum $\boldsymbol{k}_F$ at the antinode are shown in Fig. 3. The gap size is estimated from peak top energy in EDC. Though this measurement was performed under superconducting state, we think the gap-like structure at antinodal region is due to the pseudogap, since the pseudogap that opens above T_c was reported to persist at low temperature below T_c.[18] It is clearly shown that the size of the pseudogap increased with decreasing hole concentration. This fact is consistent with previously reported data.[18,22,30]

The superconducting critical temperature T_c of our samples is plotted as a function of p in Fig. 4. The samples have a wide carrier-concentration range from slightly overdoped to heavily underdoped. The carrier range of the superconducting phase in La-Bi2201 is obviously extended towards higher hole concentration compared to other cuprate superconductors.[31] The carrier concentration of the optimally doped La-Bi2201 sample was $p \sim 0.3$ holes/Cu, which is definitely larger than that of the other cuprate superconductors, $p \sim 0.16$. This large hole concentration of the optimally doped sample

is closely related both with the small superconducting gap and rather large pseudogap of La-Bi2201. This will be discussed in more detail based on the laser ARPES results later.

We performed the laser-ARPES measurements for 9 different samples. The laser-ARPES spectra $I(\boldsymbol{k},\varepsilon)$ measured for OD28 below 6 K are shown in Fig. 5a as typical examples. The Fermi vectors $\boldsymbol{k}_F$ were determined from the peak in the momentum distribution curve at the chemical potential, $I(\boldsymbol{k},\mu)$ (Fig. 5b). The energy distribution curve $I(\boldsymbol{k}_F, \varepsilon)$ of the determined $\boldsymbol{k}_F$ was extracted from $I(\boldsymbol{k},\varepsilon)$ (Fig. 5c), and converted into a symmetrized spectrum $I_{sym}(\boldsymbol{k}_F, \varepsilon) = I(\boldsymbol{k}_F, \varepsilon)+ I(\boldsymbol{k}_F, -\varepsilon)$, which is free from the Fermi-Dirac distribution function. The resulting spectra $I_{sym}(\boldsymbol{k}_F, \varepsilon)$ are plotted as a function of energy in Fig. 6. In the normal state, we should have a single peak in I_{sym} $(\boldsymbol{k}_F, \varepsilon)$ exactly at the chemical potential. However, the two peaks were clearly observed in all $I_{sym}(\boldsymbol{k}_F, \varepsilon)$ spectra except for those at $\theta = 45$ °. This fact unambiguously indicates the presence of a superconducting gap. Here θ represents the Fermi surface angle, and $\theta = 45°$ and 0° represent the nodal and antinodal directions, respectively. Obviously the gap becomes wider with deviating from $\theta = 45$ °.

In order to investigate the characteristics of superconducting gap in more detail, we plotted the experimentally observed superconducting gap as a function of $\cos(2\theta)$ in Fig. 7. In the measured range of $\cos(2\theta)$, the values of Δ were proportional to $\cos(2\theta)$ regardless of the carrier concentrations. This fact clearly indicates that, even for the heavily underdoped samples, the superconducting gap near the node is well described by the simplest *d*-wave function, $\Delta(\theta) = \Delta_0|\cos(2\theta)|$. Recently, a *d*-wave function with a "next-higher-harmonic" term was reported for underdoped $Bi_2Sr_2CaCu_2O_{8+\delta}$

(Bi2212).[32] In our nodal Bi2201 data, however, the "next-higher-harmonic" term was not found even in heavily underdoped region. The structural difference between Bi2201 and Bi2212 might be responsible for this difference in the shape of superconducting gap. However we cannot deny the presence of the "next-higher-harmonic" term in Bi2201 because we did not estimate the gap-width near the anti-nodal region. The momentum range of high-resolution laser ARPES-measurements does not cover the Fermi surface near the anti-nodal region, and the rather low energy-resolution of synchrotron ARPES measurements prevented us from clearly estimating the gap size.

The magnitude of Δ_0 that represents the strength of pairing was deduced by the function fitting for the experimentally determined $\Delta(\theta)$. Figure 8a shows the superconducting gap Δ_0 as a function of hole concentration p. We found that the $\Delta_0(p)$ increases with decreasing hole concentration in the overdoped conditions and starts to decrease after possessing a plateau that extends over a relatively wider carrier concentration of $0.16 < p < 0.26$. This fact definitely indicates that the pairing of electrons is strong not only at a particular carrier concentration but also in a rather broad range of carrier concentration.

4. Discussions

Now we are ready to discuss the carrier concentration dependence of superconducting gap and pseudogap of the present Bi2201 samples together with their relation to the critical temperature of the superconducting state. It was clearly revealed, in this study, that the superconducting gap becomes smaller with decreasing hole concentration in the heavily underdoped conditions. By superimposing carrier

concentration dependence of T_c in Fig.8a, two characteristics are noticeable. In the overdoped region, both Δ_0 and T_c increased with decreasing hole concentration. In the underdoped region, the superconducting gap kept increasing to a maximum value of Δ_0, with decreasing hole concentration, though T_c decreased. In the heavily underdoped region, T_c decreases more rapidly than Δ_0 with decreasing p. These behaviors suggest that the pseudogap that develops with decreasing hole concentration contributes to the reduction of the superconducting temperature in the underdoped region, as expected from the two-gap scenario.

In order to shed more light on the effect of pseudogap on the critical temperature, we plot $2\Delta_0/(k_BT_c)$ as a function of p in Fig. 8b. The value of $2\Delta_0/(k_BT_c)$ is about 9 for the heavily overdoped condition of $p = 4.2$ and has almost the same value in overdoped regime. Notably this value is almost the same as that of the optimally doped Bi2212 and Bi2223. With decreasing hole concentration from the optimally doped condition, $2\Delta_0/(k_BT_c)$ drastically increases and eventually reaches about 28, roughly three times as large as that of $p = 4.2$ sample. We think that this behavior results from the decrease of T_c that is caused by the development of pseudogap independently to the superconducting gap.

We also estimated the hole concentration dependence of pseudogap $\Delta_{PG}(p)$ from the synchrotron ARPES data (Fig. 3). As it was previously reported,[18,22,30] the magnitude of $\Delta_{PG}(p)$ drastically increased with decreasing hole concentration, similar to the behavior of $2\Delta_0/(k_BT_c)$. It is, therefore, natural to think that the development of pseudogap with decreasing hole concentration reduces the number of Cooper-pairs and,

consequently, reduces the critical temperature of superconducting phase. This scenario clearly accounts for the carrier concentration dependence of $2\Delta_0/(k_B T_c)$.

It is also noticeable that the largest value of Δ_0 of the present La-Bi2201 samples is much smaller than those previously reported for Bi2212 possessing a higher critical temperature.[33] This fact clearly indicates that even if the pseudogap were absent from the Bi2201, its superconducting transition temperature should be lower than that of Bi2212. By using the value $2\Delta_0/(k_B T_c) = 9$ that was observed for our heavily over doped sample where the pseudogap was almost absent, we estimated the highest T_c observable under the hypothetical condition of pseudogap-free. The resulting value was $T_c \sim 50$ K, indeed much lower than the critical temperature of Bi2212 and Bi2223.

The smaller Δ_0 in Bi2201 than that of Bi2212 or Bi2223 presumably indicates the pair-formation-energy is weaker in Bi2201. The reason why the superconducting gap of Bi2201 is smaller than that of Bi2212 and Bi2223 has not been understood yet. It may be related with the out-of-plane disordering in La-Bi2201 caused by the random distribution of La in the Sr-site. The presence of apical oxygen in both side of CuO_2 plane would enhance the influence of the disordering effect in La-Bi2201. Since both the magnitude of pseudogap and T_c were reported to be significantly affected by the ionic size of rare earth elements (RE) substituted for Sr in $Bi_2Sr_{2-x}RE_xCuO_{6+\delta}$ (RE-Bi2201),[22,34] further investigation on superconducting gap of the other series of RE-Bi2201 would help to reveal the effect of out-of-plane disorder on the superconducting gap and, consequently, on the formation of Cooper pairs. We are now in progress in performing this measurement and the result will be reported in near

future.

It would be very important to discuss the range of plateau in $\Delta_0(p)$. The presence of plateau in $\Delta_0(p)$ was also reported for $Bi_2Sr_2CuO_{8+\delta}$ samples (Bi2212). [35] The range of plateau in $\Delta_0(p)$ reported for Bi2212 was $0.75 < p < 0.20$, and that is definitely different from $0.16 < p < 0.26$ of the present samples. This fact indicates that the range of carrier concentration for stabilizing superconducting phase possesses weak but finite crystal structure dependence. We should mention also that the p-width of plateau $\Delta p_{\text{plateau}}$ of Bi2201 and Bi2212 possess almost the same value at $\Delta p_{\text{plateau}} \sim 0.1$. Despite that the mechanism leading to the difference in the range and width of plateau has not been revealed yet, the detailed comparison of structure, the range of plateau, the size of Δ_0, and the width of $\Delta p_{\text{plateau}}$ would be of great importance to understand the condition of maximum T_c.

5. Conclusion

The carrier concentration dependence of superconducting gap was investigated for a series of $Bi_2(Sr,La)_2CuO_{6+\delta}$ superconductors of various hole concentrations by means of ultra-high-resolution laser induced angle resolved photoemission spectroscopy. We found that the simple d-wave gap, $\Delta(\theta) = \Delta_0|\cos(2\theta)|$, persists even in the heavily underdoped samples. The magnitude of Δ_0 decreases with decreasing hole concentration after taking a plateau of maximum value of Δ_0 that extends over a relatively wide hole concentration range. The critical temperature of superconducting phase $T_c(p)$ decreases more drastically than $\Delta_0(p)$ with decreasing hole concentration. It is therefore confidently argued that the decreasing Δ_0 and the development of pseudogap

constructively cause the drastic reduction of T_c with decreasing hole concentration at the underdoped region.

References

1) T. Timusk and B. Statt, Rep. Prog. Phys. **62**, 61 (1999).

2) M. R. Norman, D. Pines, and C. Kallin, Advances in Physics, **54**, 715 (2005).

3) S. Huffner, M. A. Hossain, A. Damascelli, and G. A. Sawatzky, Rep. Prog. Phys. **71**, 062501 (2008).

4) V. J. Emery and S. A. Kivelson, Nature **374**, 434 (1995).

5) C. M. Varma, Phys. Rev. B **55**, 14554 (1997).

6) S. Chakravarty, R. B. Laughlin, D. K. Morr, and Chetan Nayak, Phys. Rev. B **63**, 094503 (2001).

7) A. Kanigel, M. R. Norman, M. Randeria, U. Chatterjee, S. Souma, A. Kaminski, H. M. Fretwell, S. Rosenkranz, M. Shi, T. Sato, T. Takahashi, Z. Z. Li, H. Raffy, K. Kadowaki, D. Hinks, L. Ozyuzer, and J. C. Campuzano, Nature Phys. **2**, 447 (2006).

8) T. Valla, A. V. Fedorov, Jinho Lee, J. C. Davis, and G. D. Gu, Science **314**, 1914 (2006).

9) J. Wei, Y. Zhang, H. W. Ou, B. P. Xie, D. W. Shen, J. F. Zhao, L. X. Yang, M. Arita, K. Shimada, H. Namatame, M. Taniguchi, Y. Yoshida, H. Eisaki, and D. L. Feng, Phys. Rev. Lett. **101**, 097005 (2008).

10) J. Meng, W. Zhang, G. Liu, L. Zhao, H. Liu, X. Jia, W. Lu, X. Dong, G. Wang, H. Zhang, Y. Zhou, Y. Zhu, X. Wang, Z. Zhao, Z. Xu, C. Chen, and X. J. Zhou, Phys. Rev. B **79**, 024514 (2009).

11) K. Nakayama, T. Sato, Y. Sekiba, K. Terashima, P. Richard, T. Takahashi, K. Kudo, N. Okumura, T. Sasaki, and N. Kobayashi, Phys. Rev. Lett. **102**, 227006 (2009).

12) M. Shi, J. Chang, S. Pailhes, M. R. Norman, J. C. Campuzano, M. Mansson, T. Claesson, O. Tjernberg, A. Bendounan, L. Patthey, N. Momono, M. Oda, M. Ido, C. Mudry, and J. Mesot, Phys. Rev. Lett. **101**, 047002 (2008).

13) K. Tanaka, W. S. Lee, D. H. Lu, A. Fujimori, T. Fujii, Risdiana, I. Terasaki, D. J. Scalapino, T. P. Devereaux, Z. Hussain, and Z. X. Shen, Science **314**, 1910 (2006).

14) T. Kondo, T. Takeuchi, A. Kaminski, S. Tsuda, and S. Shin, Phys. Rev. Lett. **98**, 267004 (2007).

15) K. Terashima, H. Matsui, T. Sato, T. Takahashi, M. Kofu, and K. Hirota, Phys. Rev. Lett. **99**, 017003 (2007).

16) W. S. Lee, I. M. Vishik, K. Tanaka, D. H. Lu, T. Sasagawa, N. Nagaosa, T. P. Devereaux, Z. Hussain, and Z.-X. Shen, Nature **450**, 81 (2007).

17) J.-H. Ma, Z.-H. Pan, F. C. Niestemski, M. Neupane, Y.-M. Xu, P. Richard, K. Nakayama, T. Sato, T. Takahashi, H.-Q. Luo, L. Fang, H.-H. Wen, Ziqiang Wang, H. Ding, and V. Madhavan, Phys. Rev. Lett. **101**, 207002 (2008).

18) T. Kondo, R. Khasanov, T. Takeuchi, J. Schmalian, and A. Kaminski, Nature **457**, 296 (2008).

19) R. H. He, K. Tanaka, Sung-Kwan Mo, T. Sasagawa, M. Fujita, T. Adachi, N. Mannella, K. Yamada, Y. Koike, Z. Hussain, and Z. X. Shen, Nature Phys. **5**, 119 (2008).

20) M. Hashimoto, T. Yoshida, A. Fujimori, D.H. Lu, Z.-X. Shen, M. Kubota, K. Ono, M. Ishikado, K. Fujita, and S. Uchida, Phys. Rev. B **79**, 144517 (2009).

21) T. Yoshida, M. Hashimoto, S. Ideta, A. Fujimori, K. Tanaka, N. Mannella, Z.

Hussain, Z.-X. Shen, M. Kubota, K. Ono, S. Komiya, Y. Ando, H. Eisaki, and S. Uchida, Phys. Rev. Lett. **103**, 037004 (2009).

22) Y. Okada, T. Kawaguchi, M. Ohkawa, K. Ishizaka, T. Takeuchi, S. Shin, and H. Ikuta, Phys. Rev. B **83**, 104502 (2011).

23) T. Kiss, T. Shimojima, K. Ishizaka, A. Chainani, T. Togashi, T. Kanai, X.-Y. Wang, C.-T. Chen, S. Watanabe, and S. Shin, Rev. Sci. Instrum. **79**, 023106 (2008)

24) T. Kondo, T. Takeuchi, U. Mizutani, T. Yokoya, S. Tsuda, and S. Shin, Phys. Rev. B **72**, 024533 (2005)

25) T. Takeuchi, A. Yamamoto, K. Ogawa, MRS Proc. **1314**, (2011). (DOI:10.1557/opl.2011.513)

26) Z. Konstantinovic´, G. Le Bras, A. Forget, D. Colson, F. Jean, G. Collin, Z. Z. Li, H. Raffy, and C. Ayache, Europhys. Lett. **62**, 257 (2003).

27) S. D. Obertelli, J. R. Cooper, and J. L. Tallon, Phys. Rev. B **46**, 14928 (1992)

28) P. D. C. King, J. A. Rosen, W. Meevasana, A. Tamai, E. Rozbicki, R. Comin, G. Levy, D. Fournier, Y. Yoshida, H. Eisaki, K. M. Shen, N. J. C. Ingle, A. Damascelli, and F. Baumberger, Phys. Rev. Lett. **106**, 127005 (2011).

29) A. Ino, C. Kim, M. Nakamura, T. Yoshida, T. Mizokawa, A. Fujimori, Z.-X. Shen, T. Kakeshita, H. Eisaki, and S. Uchida, Phys. Rev. B **65**, 094504 (2002).

30) Y. Okada, T. Takeuchi, T. Baba, S. Shin, and H. Ikuta, J. Phys. Soc. Jpn. **77**, 074714 (2008).

31) T. Kondo, T. Takeuchi, T. Yokoya, S. Tsuda, S. Shin, U. Mizutani, J. Electron Spectrosc. Relat. Phenom. **137-140**, 663-668 (2004).

32) H. Anzai, A. Ino, M. Arita, H. Namatame, M. Taniguchi, M. Ishikado, K. Fujita, S. Ishida, and S. Uchida, Nat. Commun. **4**, 1815 (2013).

33) Vishik, I. M., Lee, W. S., He, R. H., Hashimoto, M., Hussain, Z., Devereaux, T. P., and Shen, Z. X., New J. Phys., **12**, 105008 (2010).

34) H. Eisaki, N. Kaneko, D. L. Feng, A. Damascelli, P. K. Mang, K. M. Shen, Z.-X. Shen, and M. Greven, Phys. Rev. B **69**, 064512 (2004).

35) I. M. Vishik, M. Hashimoto, Rui-Hua He, Wei-Sheng Lee, Felix Schmitt, Donghui Lu, R. G. Moore, C. Zhang, W. Meevasana, T. Sasagawa, S. Uchida, Kazuhiro Fujita, S. Ishida, M. Ishikado, Yoshiyuki Yoshida, Hiroshi Eisaki, Zahid Hussain, Thomas P. Devereaux, and Zhi-Xun Shen, Proc. Natl. Acad. Sci. U.S.A **109**, 8332–18337 (2012).

Figure captions

Figure 1

The temperature dependence of (a) Seebeck coefficient and (b) magnetic susceptibility for selected samples. Samples are labeled by a doping-level prefix, namely underdoped (UD), optimal doped (OP) or overdoped (OD), and a trailing number denoting T_c.

Figure 2

(a)~(c) Momentum-space mapping images at $\varepsilon = \mu$, obtained from synchrotron ARPES measurement for selected samples. Dots curves donate the Fermi surfaces. (d) Hole concentrations determined from (a)~(c) were plotted as functions of Seebeck coefficient at $T = 290$ K, $S(290)$.

Figure 3

(a) Solid and dots lines show the symmetrized and raw EDCs at antinodal $\boldsymbol{k}_F$ (a gray circle in (b)) obtained from synchrotron ARPES measurement. Black triangles denote the pseudogap energy, Δ_{PG}. (b) A schematic of a Brillouin-Zone quadrant. (c) The pseudogap energies were plotted as function of the hole concentration.

Figure 4

The superconducting critical temperature T_c was plotted for the samples as a function of hole concentration, p. Hole concentrations of arrowed three samples were directly

obtained from the shapes of FS (Fig.2). For the other samples, hole concentrations were estimated from $S(290)$ of them, using the liner relation in Fig.2d.

Figure 5

Laser-ARPES data of overdoped Bi2201 with T_c = 28 K at low temperatures below 6 K. (a) The laser-ARPES spectra $I(k,\varepsilon)$ along the nodal region. The vertical dots line and the horizontal solid line represent Fermi momentum, k_F and chemical potential, μ, respectively. (b) The momentum distribution curve at chemical potential, $I(k,0)$ cut from (a). Fermi vector k_F could be decided from the peak top. (c) The energy distribution curve $I(k_F, \varepsilon)$ of the determined k_F in (b).

Figure 6

The energy distribution curves $I_{sym}(\boldsymbol{k}_F, \varepsilon)$ symmetrized at μ for all samples. Black triangle donate the gap energies. Here θ represents Fermi surface angle, and $\theta = 45°$ represent the nodal region.

Figure 7

Gap sizes as functions of $|\cos(2\theta)|$. The dotted lines denote the simplest *d*-wave gap function fits, $\Delta(\theta) = \Delta_0|\cos(2\theta)|$.

Figure 8

(a) The superconducting gap Δ_0 and the critical temperature T_c and (b) $2\Delta_0/(k_B T_c)$ were

plotted as function of hole concentration, respectively.

Figures

Figure 1

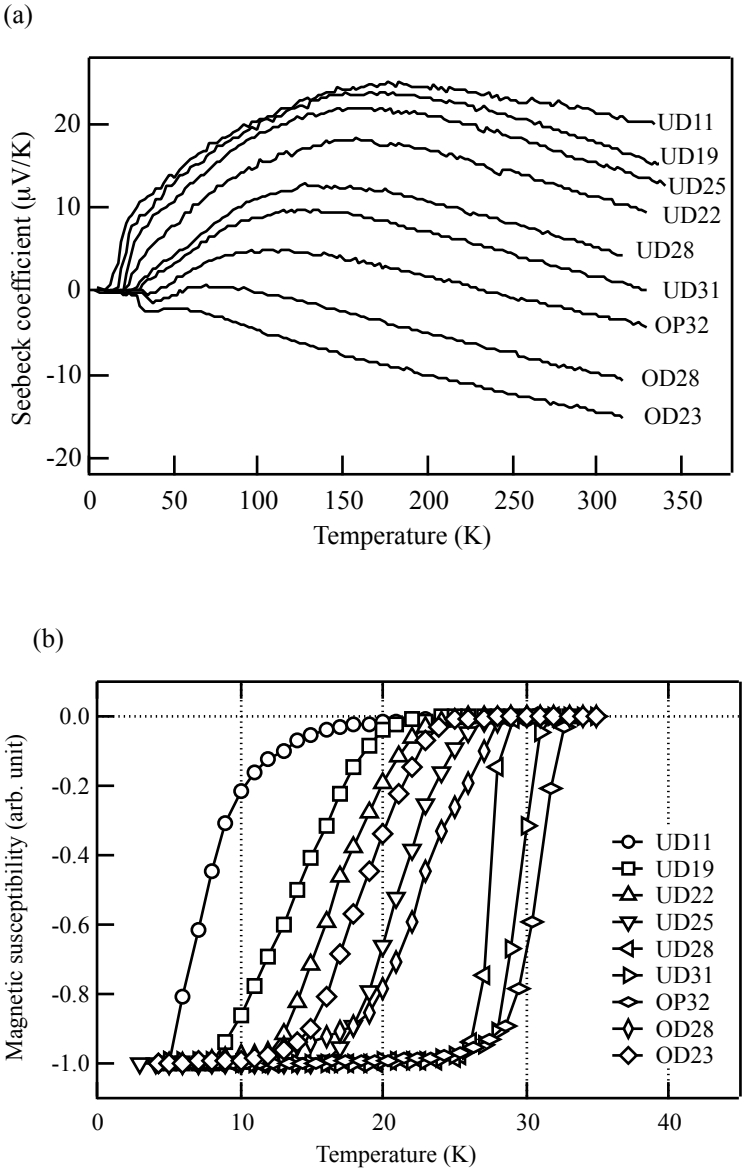

Figure 2

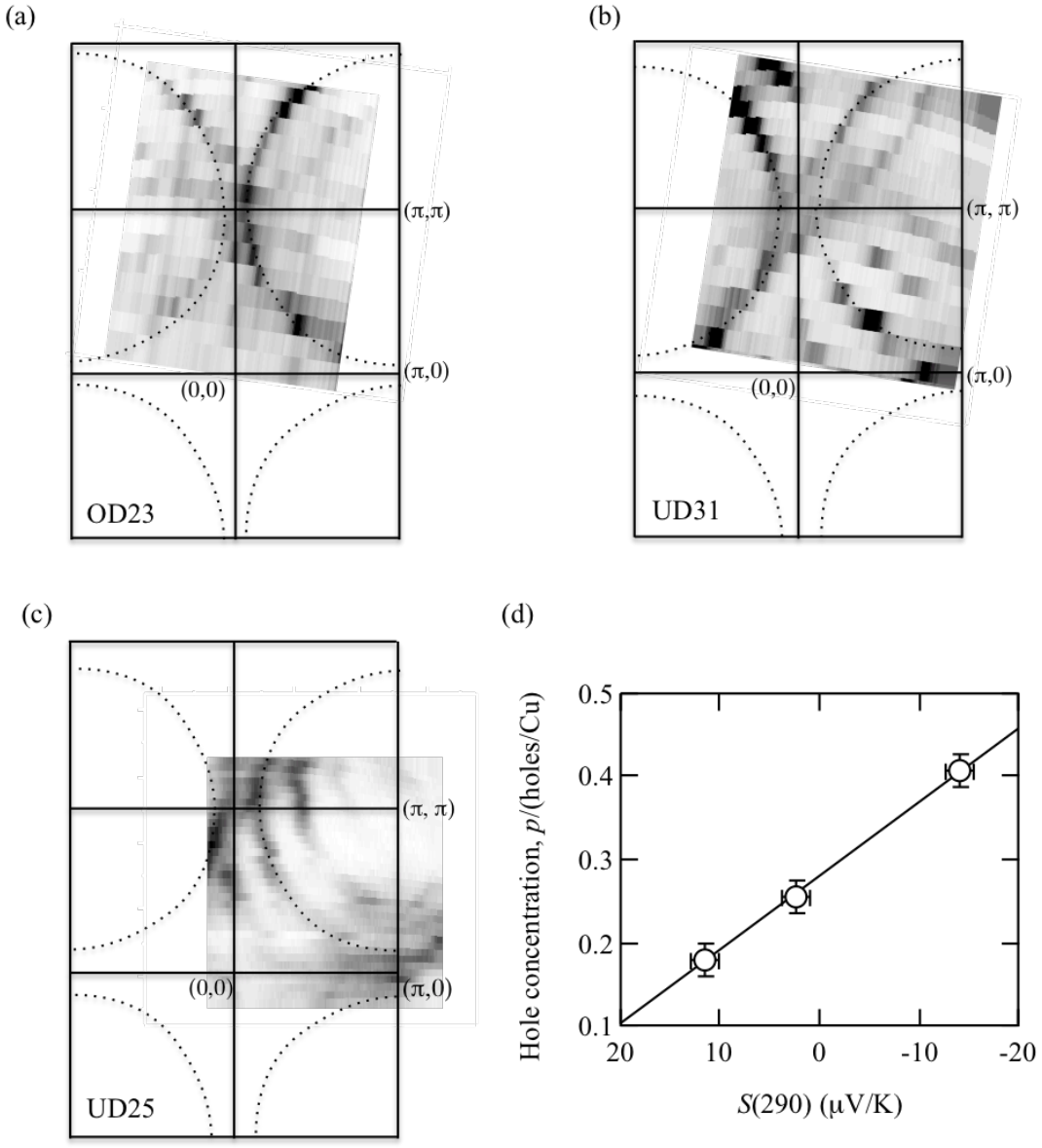
(a)
(π,π)
(π,0)
(0,0)
OD23
(b)
(π, π)
(π,0)
(0,0)
UD31
(c)
(π, π)
(0,0)
(π,0)
UD25
(d)
Hole concentration, p/(holes/Cu)
0.5
0.4
0.3
0.2
0.1
20
10
0
-10
-20
S(290) (μV/K)

Figure 3

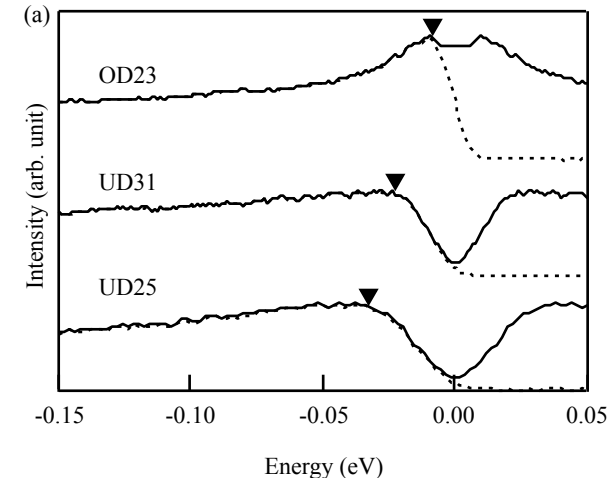
(a)
OD23
UD31
UD25
Intensity (arb. unit)
-0.15
-0.10
-0.05
0.00
0.05
Energy (eV)

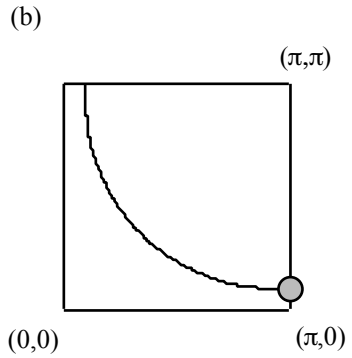
(b)
(π,π)
(0,0)
(π,0)

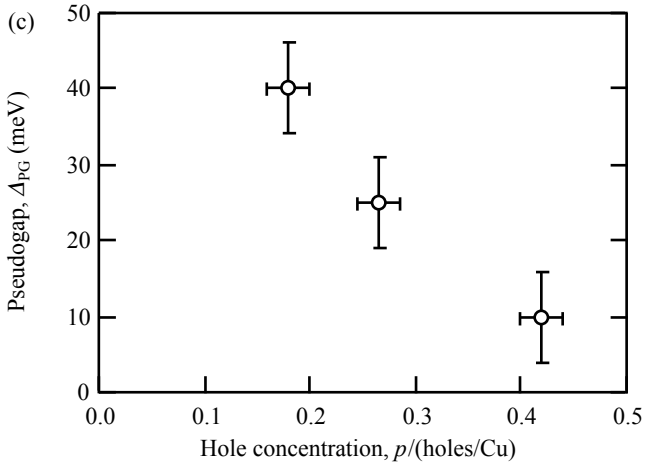
(c)
Pseudogap, Δ_{PG} (meV)
50
40
30
20
10
0
0.0
0.1
0.2
0.3
0.4
0.5
Hole concentration, p/(holes/Cu)

Figure 4

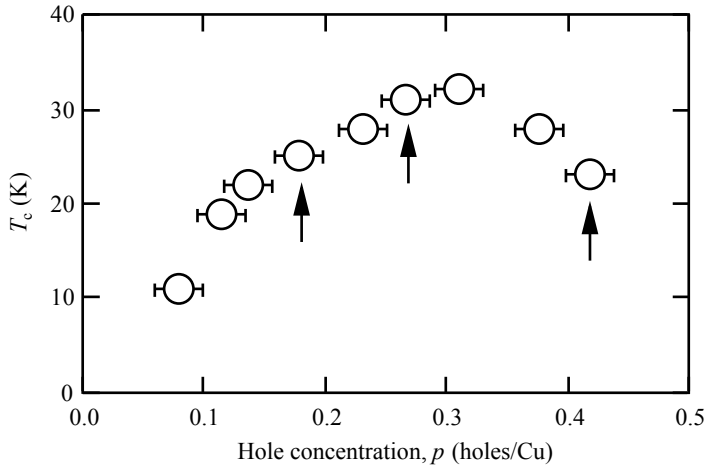

Figure 5

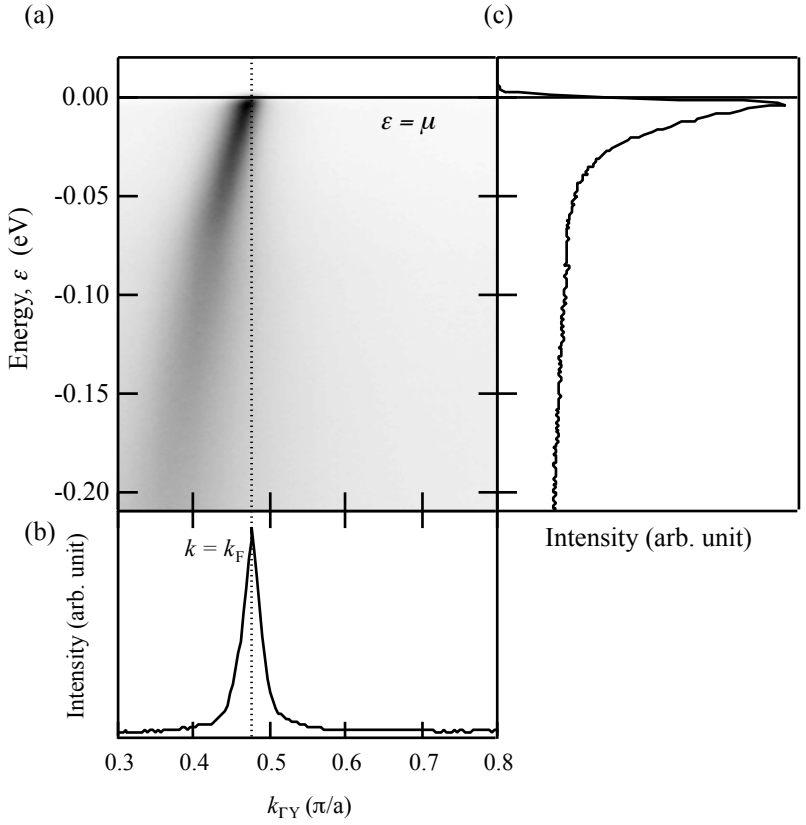

Figure 6

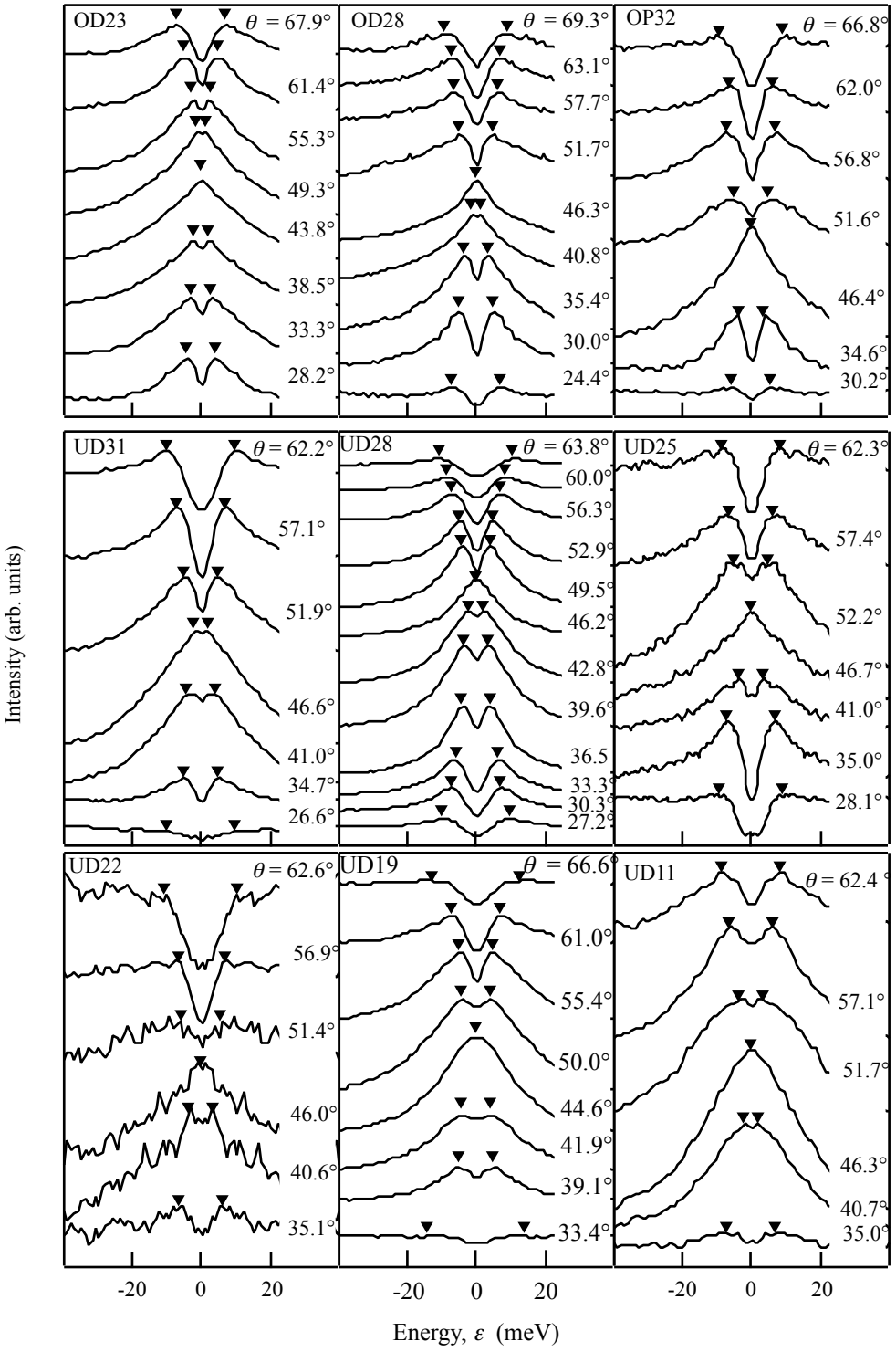
OD23
θ = 67.9°
61.4°
55.3°
49.3°
43.8°
38.5°
33.3°
28.2°
OD28
θ = 69.3°
63.1°
57.7°
51.7°
46.3°
40.8°
35.4°
30.0°
24.4°
OP32
θ = 66.8°
62.0°
56.8°
51.6°
46.4°
34.6°
30.2°
UD31
θ = 62.2°
57.1°
51.9°
46.6°
41.0°
34.7°
26.6°
UD28
θ = 63.8°
60.0°
56.3°
52.9°
49.5°
46.2°
42.8°
39.6°
36.5
33.3°
30.3°
27.2°
UD25
θ = 62.3°
57.4°
52.2°
46.7°
41.0°
35.0°
28.1°
UD22
θ = 62.6°
56.9°
51.4°
46.0°
40.6°
35.1°
UD19
θ = 66.6°
61.0°
55.4°
50.0°
44.6°
41.9°
39.1°
33.4°
UD11
θ = 62.4 °
57.1°
51.7°
46.3°
40.7°
35.0°
Intensity (arb. units)
-20
0
20
Energy, ε (meV)

Figure 7

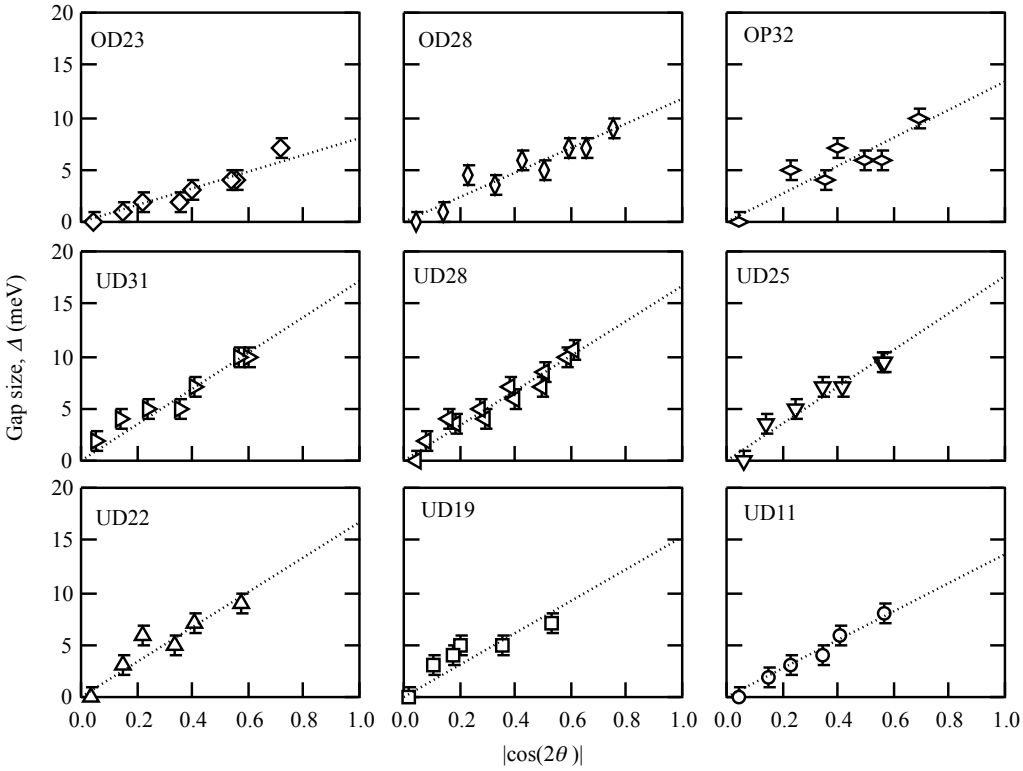
OD23
OD28
OP32
UD31
UD28
UD25
UD22
UD19
UD11
Gap size, Δ (meV)
|cos(2θ)|
0
5
10
15
20
0.0
0.2
0.4
0.6
0.8
1.0

Figure 8

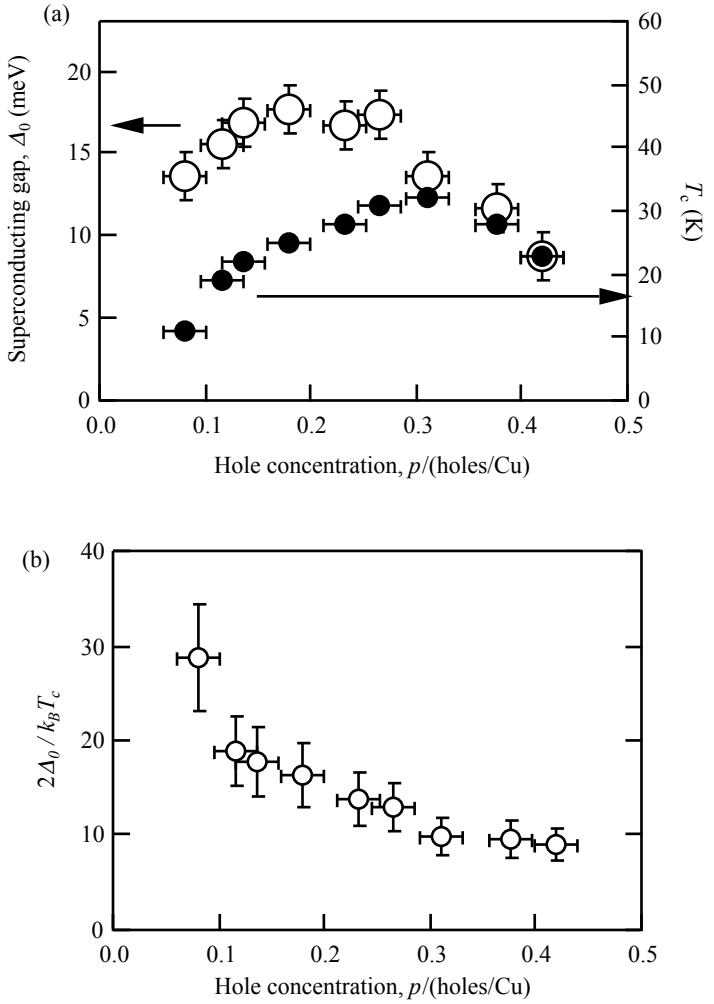
(a)
Superconducting gap, Δ_0 (meV)
T_c (K)
Hole concentration, p/(holes/Cu)
(b)
$2\Delta_0 / k_B T_c$
Hole concentration, p/(holes/Cu)